Actinic critical dimension measurement of contaminated extreme ultraviolet mask using coherent scattering microscopy

Jae Uk Lee, Seongchul Hong, Jinho Ahn, Jonggul Doh, and SeeJun Jeong

Citation: Journal of Vacuum Science & Technology B, Nanotechnology and Microelectronics: Materials, Processing, Measurement, and Phenomena **32**, 031601 (2014); doi: 10.1116/1.4873697

View online: https://doi.org/10.1116/1.4873697

View Table of Contents: http://avs.scitation.org/toc/jvb/32/3

Published by the American Vacuum Society

Actinic critical dimension measurement of contaminated extreme ultraviolet mask using coherent scattering microscopy

Jae Uk Lee, Seongchul Hong, and Jinho Ahn[a)]
Department of Materials Science and Engineering, Hanyang University, Seoul 133-791, South Korea

Jonggul Doh
Mask Development Team, Semiconductor R&D Center, Samsung Electronics, Co., Ltd., Hwasung, Gyeonggi 445-701, South Korea

SeeJun Jeong
Department of Convergence Nanoscience, Hanyang University, Seoul 133-791, South Korea

(Received 20 October 2013; accepted 16 April 2014; published 28 April 2014)

The authors evaluated the feasibility of using coherent scattering microscopy (CSM) as an actinic metrology tool by employing it to determine the critical dimension (CD) and normalized image log-slope (NILS) values of contaminated extreme ultraviolet (EUV) masks. CSM was as effective as CD scanning electron microscopy (CD-SEM) in measuring the CD values of clean EUV masks in the case of vertical patterns (nonshadowing effect); however, only the CSM could detect shadowing effect for horizontal patterns resulting in smaller clear mask CD values. Owing to weak interaction between the low-density contaminant layer and EUV radiation, the CSM-based CD measurements were not as affected by contamination as were those made using CD-SEM. Furthermore, CSM could be used to determine the NILS values under illumination conditions corresponding to a high-volume manufacturing tool. [http://dx.doi.org/10.1116/1.4873697]

I. INTRODUCTION

Critical dimension scanning electron microscopy (CD-SEM) is widely used as a metrology tool for optical masks. However, it is difficult to measure the actual CDs of extreme ultraviolet (EUV) lithography masks, given that the optical properties of the mask materials are wavelength specific and the angle of incidence of the EUV light is oblique.[1–3] Several actinic mask inspection and metrology techniques have been developed for use with EUV masks,[4–9] and mask contamination is mostly investigated through topography analysis.[10] However, there is no appropriate tool to investigate the effects of mask contamination on the imaging properties. Coherent scattering microscopy (CSM) is an actinic inspection and metrology tool that can obtain an aerial image of EUV masks using reverse Fourier transform of the diffraction pattern in conjunction with a phase retrieval algorithm.[11–16] Using CSM, one can obtain aerial images without requiring complex optics. One can also simulate imaging quality under various illumination conditions. In this study, we demonstrated the actinic metrology capability of CSM with respect to contaminated EUV masks and compared the results with those of CD-SEM.

II. EXPERIMENT

The CSM system consisted of a source chamber, in which EUV radiation was generated using a femtosecond laser, and an optics chamber for inspecting mask patterns. In the source chamber [Fig. 1(a)], an infrared femtosecond laser was reflected by a concave mirror and focused on Ne gas contained in a gas cell. The excited electrons of the Ne gas generated high-order harmonic waves that contained a 59th harmonic with a wavelength of 13.5 nm.[17–22] This harmonic was filtered by an EUV mirror and Zr spectral-purity filters. The extracted EUV radiation exhibited good spatial and temporal coherence (<0.25 mrad, $\lambda/\Delta\lambda = 294$) and a stable

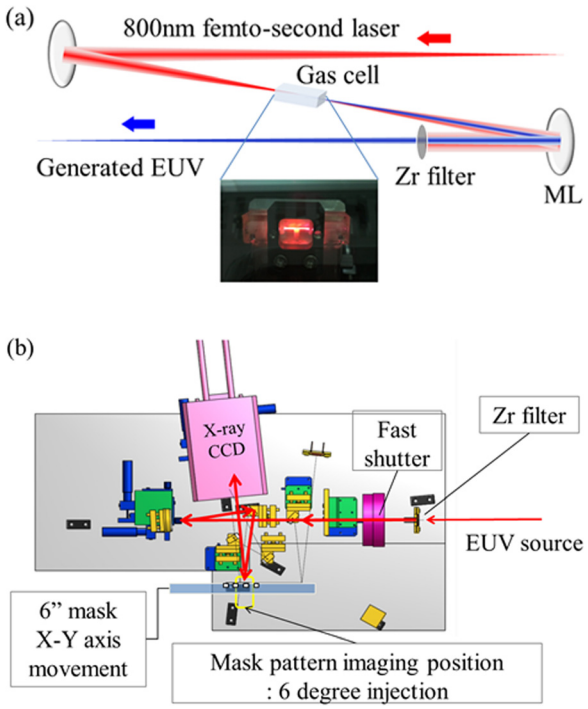

FIG. 1. (Color online) Schematic of (a) the source chamber and (b) the optic chamber.

[a)]Electronic mail: jhahn@hanyang.ac.kr

average power of 50 nW.[23] The stability of the intensity of the EUV radiation was measured and found to be 4.4% (3σ) over an operation period of 1 h. In the optics chamber [Fig. 1(b)], the EUV light was reflected by concave and plane mirrors and was focused onto the EUV mask. To ensure a field of view (FOV) of 1.5 μm, we used two concave mirrors in series to focus the EUV light. The first concave mirror, which was in the source chamber, was 1 in. in size and had a radius of curvature of 1200 mm, while the second mirror, which was in the optics chamber, was 1 in. in size and had a radius of curvature of 80 mm. The diffraction pattern from the mask was recorded with a large-area x-ray charge coupled device (CCD) with a 2048 $\times$ 2048 pixels array and pixel size of 13.5 μm $\times$ 13.5 μm.

The CSM system reconstructed the aerial image of the EUV mask pattern from the diffraction pattern captured by the CCD using an oversampling method and a phase-retrieval algorithm. Because the diffraction pattern does not have phase information, we adopted an error-reduction algorithm (ERA) and a hybrid input–output (HIO) phase-retrieval algorithm to obtain the phase information and reconstruct the aerial image. We assumed an invariant optical system in which the beam exhibits constant coherence and intensity for angles of incidence of 6° $\pm$ 2° (4°–8°). While developing the HIO algorithm, Fienup solved the problems of stagnation and convergence encountered in earlier algorithms by adopting a support constraint in the object domain.[24] The HIO support was a 2-μm-diameter circle, which was a little bigger than the beam size (1.5 μm in diameter), and the maximum numerical aperture (NA) of the CCD camera was 0.59. The HIO algorithm consists of four steps:

(1) Find the inverse Fourier transform of the diffraction pattern of the EUV mask.
(2) Apply the constraints in real space.
(3) Find the Fourier transform of the estimate of the inverse Fourier transform.
(4) Apply the Fourier constraint and substitute the modulus of the measured amplitude.

These four steps were repeated iteratively until the required precision was achieved. Figure 2 shows a schematic of the iterative phase-retrieval algorithm. When only the ERA was used for image reconstruction, we experienced the problem of a local minimum, as shown in Fig. 3. In this case, it did not yield a higher-quality reconstructed image even when the number of iterations was increased. However, the HIO algorithm was able to overcome this issue. Figure 4 shows the reconstructed images and CD profiles obtained after different number of iterations of the HIO algorithm. The CD profile was measured at the cross line of the center of the reconstructed line image. The reconstructed image changed gradually as the number of iterations was increased, approaching the detected image. However, the reconstructed image did not change much after the 10th iteration, and we adopted 10th iteration image for experimental result. The repeatability of the CD measurement of a 78 nm line and space (L/S) pattern was 0.3 nm (3σ); this was determined after making 50 measurements in a 20 min period.[25]

Binary EUV masks with 70-nm-thick TaN absorber layer were fabricated on a Ru-capped reflector consisting of 40 pairs of Mo/Si multilayers (ML). EUV masks with 88, 100, and 128 nm half-pitch L/S patterns were produced. In order to test the effects of contamination, the EUV masks were intentionally contaminated with carbon in an EUV contamination chamber at Pohang Accelerator Laboratory. The masks were coated with an approximately 20-nm-thick carbon layer; the thickness of the layer was measured using atomic force microscopy (AFM), and the measurements were performed over a 500-μm-wide area. The CD values of the contaminated masks were measured using a Leica 9045 CD-SEM system and the above-described CSM system.

III. RESULTS AND DISCUSSION

In order to investigate the feasibility of using CSM as a metrology tool, we compared the reconstructed CSM images and the CD-SEM images of uncontaminated EUV masks with L/S patterns with half pitches of 88, 100, and 128 nm. CSM determines mask CD values on the basis of rigorous coupled-wave analysis (RCWA) method, which is based on Maxwell's equations, making use of the measured diffraction pattern. The library of mask CD values is generated using a mask CD model, which is fitted using the intensity of the diffraction patterns measured through CSM. The mask

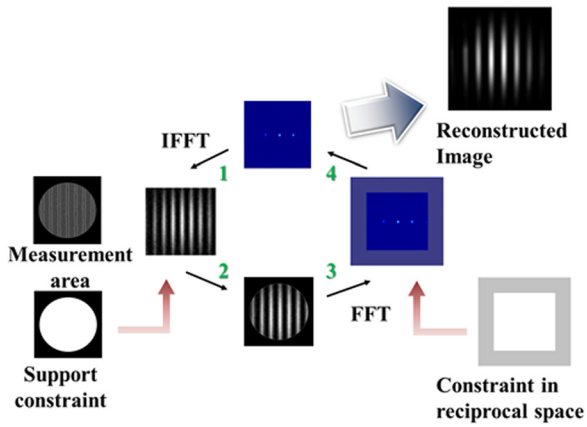

FIG. 2. (Color online) Schematic of the iterative phase-retrieval algorithm.

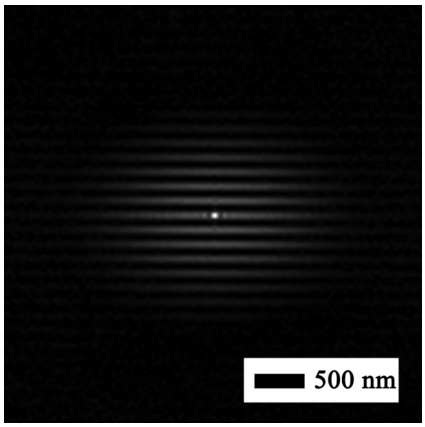

FIG. 3. Local minimum image obtained using the ERA.

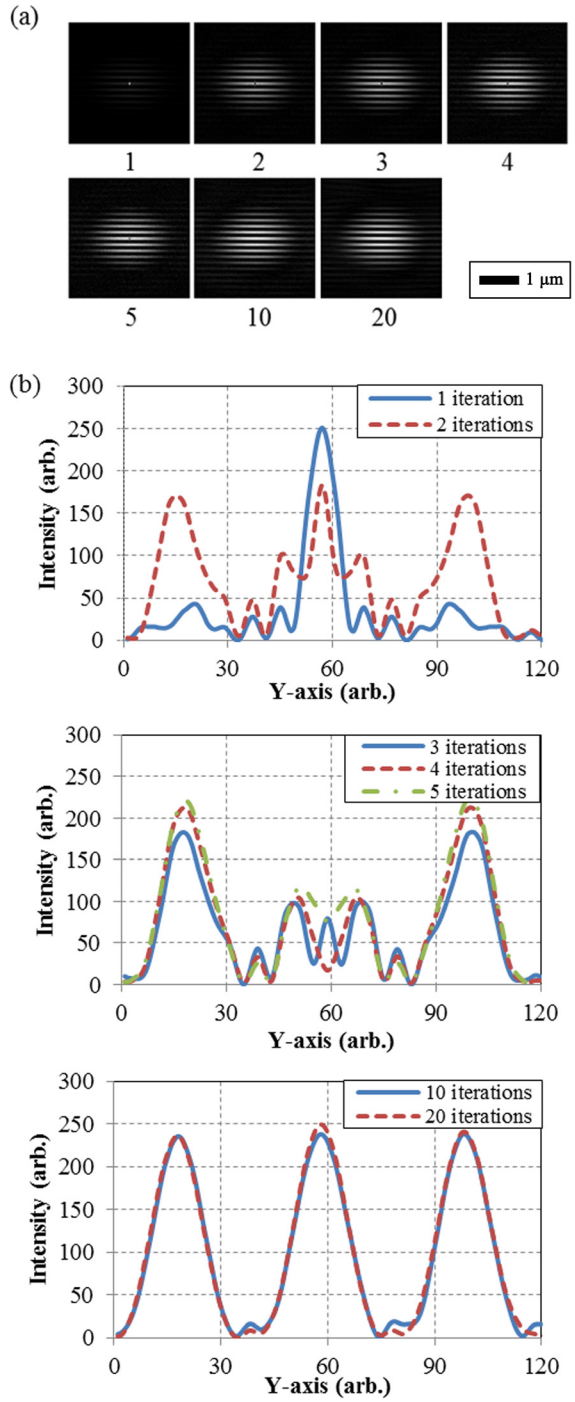

FIG. 4. (Color online) (a) Image reconstruction after several iterations of the HIO algorithm and (b) CD profiles after 1, 2, 3, 4, 5, 10, and 20 iterations of the HIO algorithm.

CD values measured using CSM were similar to the values measured using CD-SEM. As can be seen from Fig. 5, CSM and CD-SEM images were well matched for vertical patterns, because there is no shadowing effect altering CD values measured using CSM. In order to confirm the feasibility of CSM as a mask metrology tool, we compared the CD maps for clear masks with 128 nm L/S patterns (Fig. 6). The CSM results exhibited a good correlation with the CD-SEM measurements in the case of the vertical patterns (the difference in the average values was 0.3 nm); however, in the case

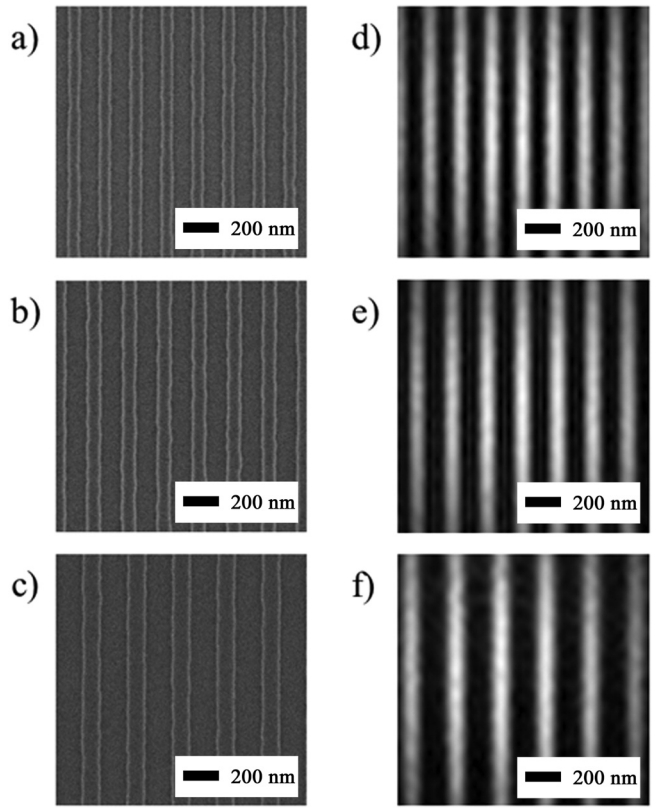

FIG. 5. CD-SEM images of (a) 88 nm, (b) 100 nm, and (c) 128 nm L/S patterns of EUV masks and CSM images (vertical patterns) of (d) 88 nm, (e) 100 nm, and (f) 128 nm L/S patterns of EUV masks.

of the horizontal patterns, the clear mask CD values measured by CSM were lower, owing to the shadowing effect.[26–31] The horizontal and vertical patterns were both measured at the best focus. Here, the horizontal–vertical (H–V) CD bias of the mask was 7.1 nm. This value is smaller than that attributable to the geometrical shadowing effect predicted by the following equation:[32]

$$2 \times T_{abs} \times \tan(6^\circ) = 14.7 \text{ nm}, \quad (1)$$

where T_{abs} is the thickness of the absorber layer and 6° is the angle of incidence of the EUV light. We believe CSM yields the actual aerial CD value by emulating an exposure tool with an angle of incidence of 6°. We investigated the effect of contamination on the mask CD values using several

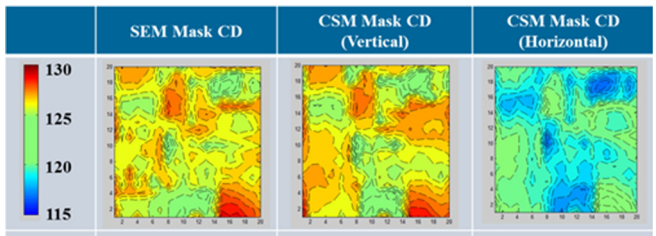

	SEM Mask CD	CSM Mask CD (Vertical)	CSM Mask CD (Horizontal)
Max	129.7	128.8	122.5
Min	123.6	124.4	117.1
Avg.	126.3	126.6	119.5
CDU (3σ)	2.9	3.7	3.0

FIG. 6. (Color online) CD maps measured using CSM and CD-SEM.

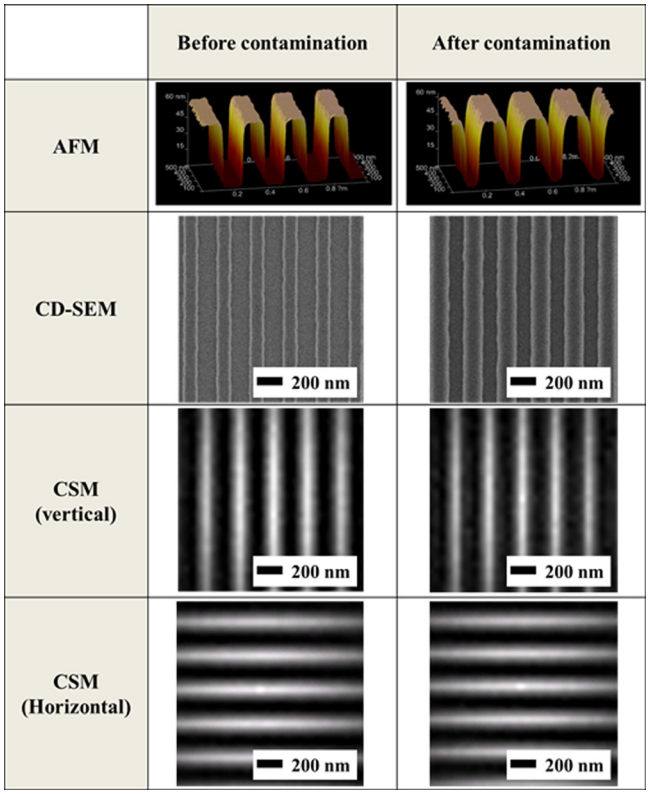

FIG. 7. (Color online) Vertical AFM profiles, CD-SEM images, and vertical and horizontal CSM images of an EUV mask with 128 nm L/S patterns before and after carbon contamination.

techniques (Fig. 7, Table I). To determine the reliability of the mask CD measurements made using CSM, both clean and contaminated areas were measured at the same time and under similar exposure conditions (500 ms, 3 accumulations) in a vacuum chamber. Using AFM to measure mask CD values resulted in decreased space widths (or increased line widths) and increased absorber layer thickness. While the changes in the mask CD value owing to contamination were similar when measured using CD-SEM and AFM (36.3 and 35.1 nm, respectively), the change in the CD value of vertical patterns as measured using CSM was much smaller (19.4 nm). Furthermore, the H–V CD bias in the case of the contaminated mask was small as well (0.3 nm); this value is much smaller than the value measured before contamination (7.1 nm). We believe that these results are due to the low-density carbon contamination with much lower EUV absorption coefficient than TaN absorber ($k_{Carbon} = 0.0069$, $k_{TaN} = 0.0446$). The weak optical interference of EUV radiation by low-density carbon layer results in a smaller CD variation due to contamination in CSM compared to CD-SEM and AFM.[33,34] CD-SEM and AFM can only measure the physical thickness of contaminant layer; on the other hand, with CSM, one can detect the actual optical effects of the contaminant layer at EUV wavelengths.

TABLE I. Measurement of CD values of an EUV mask before and after contamination (values in nm).

Measurement Tool	AFM	CD-SEM	CSM (vertical)	CSM (horizontal)
Before contamination	142.9	144.6	151.6	144.8
After contamination	107.8	108.3	132.2	131.9
Difference in CD value	35.1	36.3	19.4	12.9

To compare the quality of the aerial images obtained before and after contamination, the normalized image log-slope (NILS) values were determined under illumination condition of a high-volume manufacturing tool (NA = 0.33, $\sigma = 0.9$, conventional illumination). We designated the intensity threshold levels of the aerial image CD values to be one-fourth the CD values of the masks with L/S values of 88, 100, and 128 nm, as the demagnification factor was 1/4. The threshold levels were 51%, 48%, and 45%, respectively. The CD values of the aerial images were measured at these threshold levels. We calculated the NILS values by measuring the slope at the point of CD measurement in the intensity profile of the reconstructed image. The NILS, which

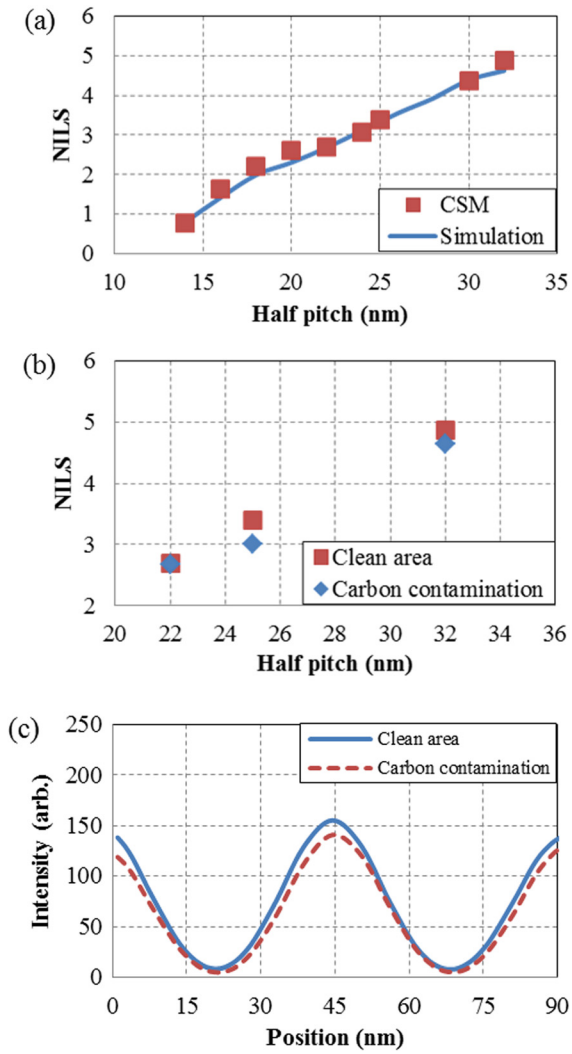

FIG. 8. (Color online) (a) NILS values obtained on the basis of the field spectrum using CSM and simulations performed using EM-SUITE (NA = 0.33, $\sigma = 0.9$, conventional illumination), (b) NILS values of the clean and contaminated areas, (c) aerial image profiles of clean and contaminated masks with 100 nm half-pitch L/S patterns.

describes the quality of aerial images for lithographic processes, is defined as follows:

$$\mathrm{NILS} = \mathrm{CD} \times \mathrm{ILS} = \mathrm{CD}\frac{1}{\mathrm{I}}\frac{\mathrm{dI}}{\mathrm{dx}} = \mathrm{CD}\frac{\mathrm{d}\ \ln(\mathrm{I})}{\mathrm{dx}}, \qquad (2)$$

where I is the intensity of the aerial image. The NILS values for the L/S patterns of the clean masks as measured by CSM were consistent with the results of simulations performed using the software EM-SUITE,[35] as can be seen from Fig. 8(a). As anticipated, carbon contamination decreased the NILS values of the aerial images. As shown in Fig. 8(b), the NILS values were reduced from 2.7, 3.39, and 4.78 to 2.66, 3.1, and 4.64 for the 88, 100, and 128 nm L/S half-pitch patterns, respectively. Further, as can be seen from Fig. 8(c), the image profiles obtained using CSM confirmed that the decrease in the NILS values was caused primarily by the decrease in the maximum intensity of the images, which was the result of the carbon contamination.

IV. SUMMARY AND CONCLUSIONS

In this study, we employed CSM as an actinic metrology tool to evaluate the actual optical performance of EUV masks before and after contamination. Before contamination, in the case of vertical patterns, CSM resulted in mask CD values similar to those obtained using CD-SEM; however, the clear mask CD values obtained using CSM for horizontal patterns on uncontaminated masks were lower, owing to the shadowing effect. In the case of the contaminated masks, the absolute clear mask CD values and the change in the mask CD values owing to contamination as measured using CSM were lower than those obtained using CD-SEM and AFM. This is because CSM can detect the weak optical interaction between the low-density contaminant layer and the EUV radiation. CSM showed reduced NILS value after contamination. Therefore, we believe that CSM can be a powerful actinic metrology tool for evaluating EUV masks.

ACKNOWLEDGMENTS

This work was supported by the Basic Science Research Program through a National Research Foundation of Korea (NRF) grant funded by the Korean Government (MEST) (Grant No. 2011-0028570).

[1]G. Tallents, E. Wagenaars, and G. Pert, Nat. Photonics **4**, 809 (2010).
[2]M. Sugawara, A. Chiba, and I. Nishiyama, J. Vac. Sci. Technol. B **21**, 2701 (2003).
[3]M. Sugawara, M. Ito, T. Ogawa, E. Hoshino, A. Chiba, and S. Okazaki, J. Microlithogr., Microfabr., Microsyst. **2**, 27 (2003).
[4]K. A. Goldberg and I. Mochi, J. Vac. Sci. Technol. B **29**, 06F502 (2011).
[5]K. A. Goldberg, P. Naulleau, I. Mochi, E. H. Anderson, S. B. Rekawa, C. D. Kemp, R. F. Gunion, H. S. Han, and S. Huh, J. Vac. Sci. Technol. B **26**, 2220 (2008).
[6]I. Mochi, K. A. Goldbergm, and S. Huh, J. Vac. Sci. Technol. B **28**, C6E11 (2010).
[7]T. Terasawa, T. Yamane, T. Tanaka, O. Suga, and T. Tomie, Jpn. J. Appl. Phys. **49**, 06GD02 (2010).
[8]K. Takase *et al.*, Jpn. J. Appl. Phys. **49**, 06GD07 (2010).
[9]H. Kinoshita, T. Yoshizumi, M. Osugi, J. Kishimoto, T. Sugiyama, T. Uno, and T. Watanabe, Microelectron. Eng. **86**, 505 (2009).
[10]Y. J. Fan *et al.*, Proc. SPIE **7636**, 76360G (2010).
[11]T. Harada, M. Nakasuji, M. Tada, Y. Nagata, T. Watanabe, and H. Kinoshita, Jpn. J. Appl. Phys., Part 1 **50**, 06GB03 (2011).
[12]J. Miao, T. Ishikawa, E. Anderson, and K. Hodgson, Phys. Rev. B **67**, 174104 (2003).
[13]J. Miao, D. Sayre, and H. N. Chapman, J. Opt. Soc. Am. **15**, 1662 (1998).
[14]R. Sandberg *et al.*, Phys. Rev. Lett. **99**, 098103 (2007).
[15]T. S. H. Takajo, T. Takahashi, and S. Takahata, Appl. Opt. **38**, 5568 (1999).
[16]J. Miao, T. Ishikawa, B. Johnson, E. Anderson, B. Lai, and K. Hodgson, Phys. Rev. Lett. **89**, 088303 (2002).
[17]D. Lee, J. Kim, K. Hong, and C. Nam, Phys. Rev. Lett. **87**, 243902 (2001).
[18]M. Kakehata, H. Takada, K. Miyazaki, H. Kono, I. Kawata, and Y. Fujimura, Appl. Phys. B **70**, 219 (2000).
[19]E. Takahashi, Y. Nabekawa, T. Otsuka, M. Obara, and K. Midorikawa, Phys. Rev. A **66**, 021802 (2002).
[20]J. Choi, S. Kim, I. Y. Park, and S. W. Kim, Proc. SPIE **7757**, 77571D (2010).
[21]S. Kim, J. Jin, Y. J. Kim, I. Y. Park, Y. Kim, and S. W. Kim, Nature **453**, 757 (2008).
[22]M. C. Marconi and P. W. Wachulak, Prog. Quantum Electron. **34**, 173 (2010).
[23]D. Lee, J. Doh, H. Seo, B. Yoo, J. Choi, J. Ahn, S. Kim, and H. Cho, "Development of coherent EUV source for EUV mask metrology," *International Symposium on EUVL*, Miami, FL, 2011.
[24]J. R. Fienup, Appl. Opt. **21**, 2758 (1982).
[25]J. Doh, J. Lee, J. Ahn, and S. Kim, J. Vac. Sci. Technol. B **30**, 06F504 (2012).
[26]A. M. Myers, G. F. Lorusso, I. Kim, A. M. Goethals, R. Jonckheere, J. Hermans, B. Baudemprez, and K. Ronse, J. Vac. Sci. Technol. B **26**, 2215 (2008).
[27]G. F. Lorusso *et al.*, J. Vac. Sci. Technol. B **25**, 2127 (2007).
[28]P. C. W. Ng, K. Y. Tsai, Y. M. Lee, F. M. Wang, J. H. Li, and A. C. Chen, J. Micro/Nanolithogr. MEMS MOEMS **10**, 013004 (2011).
[29]T. Kim, B. Kim, I. Kang, Y. Chung, J. Ahn, S. Lee, I. Park, C. Kim, and N. Lee, J. Vac. Sci. Technol. B **24**, 2820 (2006).
[30]H. Kang, S. Park, C. Hwangbo, H. Seo, S. Kim, and H. Cho, J. Nanosci. Nanotechnol. **12**, 3330 (2012).
[31]M. Yoo, Y. Jeon, J. Ahn, and H. Oh, J. Korean Phys. Soc. **46**, 1020 (2005).
[32]P. Yan, Proc. SPIE **4688**, 150 (2002).
[33]J. Doh, S. Lee, J. Lee, S. Hong, C. Jeong, D. Lee, S. Kim, and J. Ahn, Jpn. J. Appl. Phys., Part 1 **51**, 06FB04 (2012).
[34]See http://www.cxro.lbl.gov for the Center for X-Ray Optics.
[35]See http://www.panoramictech.com for Panoramic Technology.